Microscopic Origin of Random Telegraph Noise Fluctuations in Aggressively Scaled RRAM and its Impact on Read Disturb Variability

N. Raghavan[1, 2, ♣], R. Degraeve[1], A. Fantini[1], L. Goux[1], S. Strangio[1], B. Govoreanu[1], D.J. Wouters[1, 2], G. Groeseneken[1, 2] and M. Jurczak[1]

[1]Interuniversity Microelectronics Center (IMEC), Kapeldreef 75, B-3001 Heverlee, Belgium.

[2]Katholieke Universiteit Leuven (KUL), Dept. of Electrical Engineering (ESAT), Kasteelpark Arenberg 10, B-3001, Belgium.

[♣] Ph: (+32) 470 344 293, E-mail: raghan@imec.be

Abstract — **Random telegraph noise (RTN) is an important intrinsic phenomenon of any logic or memory device that is indicative of the reliability and stochastic variability in its performance. In the context of the resistive random access memory (RRAM), RTN becomes a key criterion that determines the read disturb immunity and memory window between the low (LRS) and high resistance states (HRS). With the drive towards ultra-low power memory (low reset current) and aggressive scaling to 10 × 10 nm^2 area, contribution of RTN is significantly enhanced by every trap (vacancy) in the dielectric. The underlying mechanisms governing RTN in RRAM are yet to be fully understood. In this study, we aim to decode the role of conductance fluctuations caused by oxygen vacancy transport and inelastic electron trapping and detrapping processes. The influence of resistance state (LRS, shallow and deep HRS), reset depth and reset stop voltage ($V_{RESET\text{-}STOP}$) on the conductance variability is also investigated.**

Keywords – Conductive filament, Constriction, Oxygen vacancy, Quantum point contact, Thermochemical model, Trap-Detrap, Variability.

I. INTRODUCTION

The advent of the resistive random access memory (RRAM) technology is perceived as the most suitable replacement for Flash technology in order to aggressively downscale the device size to 10 × 10 nm^2, increasing integration density and also satisfying the performance targets in terms of speed, endurance, retention lifetime etc… While various reports have demonstrated the robust performance of HfO_x based RRAM [**1**] – [**5**] in the context of the above metrics, a comprehensive insight into RTN influence on stability of memory operation is still lacking. The motivation of this study is to understand the underlying mechanisms governing RTN during switching. In order to study the phenomenon, we carry out most of our noise measurements in the HRS (smaller defect cluster), wherein the contribution of individual defects is more pronounced. It has been demonstrated using electrical measurements as well as quantum-level modeling [**6**, **7**] that the quantum point contact (QPC) scenario describes the HRS *I-V* conduction in HfO_x-based RRAM very well for moderate levels of reset. In order to describe the kinetics of ionic / vacancy transport during the switching process, the hourglass model [**8**, **9**] has also been established wherein the set and reset states are determined by the back and forth drift of oxygen vacancies between the filament and the top-bottom reservoirs (~electrodes). While the forming process and the asymmetry of the stack in terms of the oxygen scavenging ability of the two electrodes determines the shape and size of the conductive filament and the overall number of defects (fixed after forming) participating for the lifetime of the switching process, the magnitude of the SET (V_{SET}) and RESET voltage (V_{RESET}) and their polarity influence the position of the vacancies in the stack.

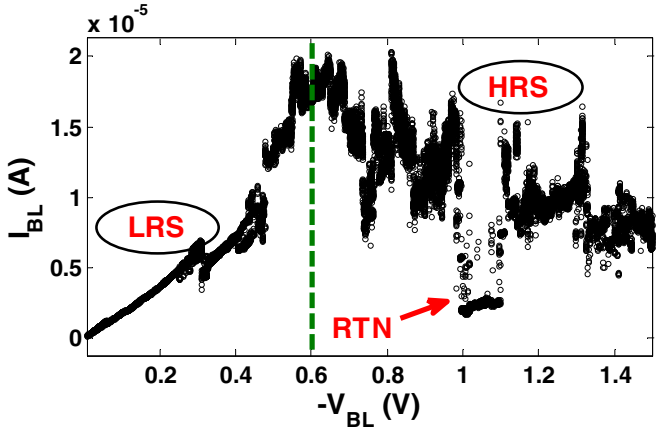

Figure 1. Trend of reset using a very slow ramp sweep of 20 mV/sec. Significant current fluctuations with large RTN steps are observed after the reset transition is triggered at around V_{BL} ~ -0.6V.

A typical trend of bipolar reset for a 5 nm HfO_x 40 × 40 nm^2 device is shown in Fig. 1 using an ultra-slow ramp sweep (20mV/sec). It may be noticed that while the LRS state shows minimal fluctuations, after the reset transition around -0.6V, significant abrupt current fluctuations along with RTN-like steps are present. These large steps are more likely to be due to the change in defect count caused by stochastic vacancy movements in and out of the filament. As shown in Figs. 2 and 3, we observe two convoluted RTN trends during the *I-V* sweep traces or at certain read voltage conditions in the HRS. The presence of two distinct signatures at different instants of the noise measurement with very different current steps (ΔI) suggests that they could be induced by the standard inelastic electron trapping and detrapping process, as observed in logic [**10**] and Flash memory stacks [**11**, **12**] and additionally, by the vacancy transport induced filament conductivity fluctuation.

978-1-4799-0113-5/13/$31.00 ©2013 IEEE

While the stochastic charge trapping phenomenon in RRAM has been well studied and confirmed for various stacks in the recent past [**13**] – [**19**], this is the first report, to our knowledge, documenting the triggering of RTN due to vacancy perturbations in the filament.

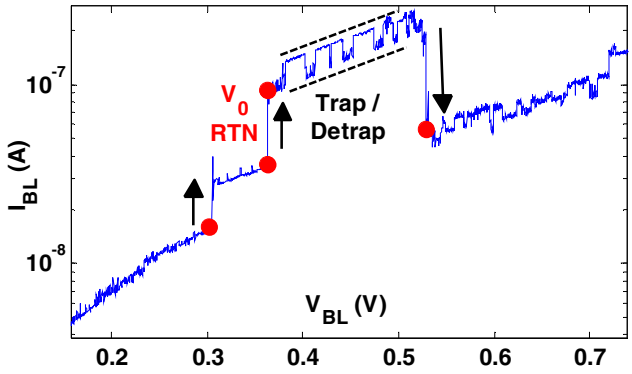

Figure 2. Observation of embedded RTN signals during a slow positive polarity ramp sweep in the HRS. The large current jumps (indicated by red dots and arrows) correspond to vacancy induced conductivity fluctuations (verified by QPC fitting for different integer number of defects) and the smaller jumps correspond to the stochastic electron trap / detrap process.

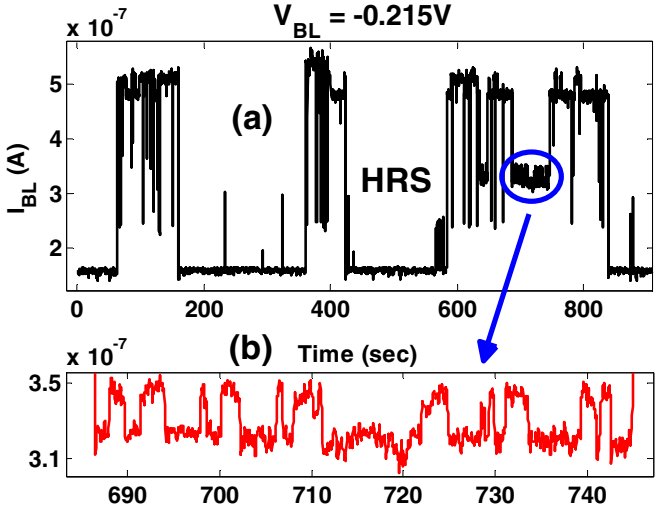

Figure 3. Constant voltage RTN measurement in HRS at V_{TE} - V_{BE} = V_{BL} – V_{SL} = -0.215V (negative polarity sensing) with transistor fully open (V_{WL} = 2V). Two different RTN patterns (smaller one evident in the zoomed in version in (b)) with almost an order of magnitude difference in ΔI values are observed.

We will present evidence using the QPC model in support of V_0-induced RTN and its detrimental role in affecting the stability of the read process in HRS. From a technology point of view, the influence of resistance state (LRS, shallow and deep reset to HRS), reset depth and reset stop voltage ($V_{RESET-STOP}$) on the conductance variability has also been probed. The depth of reset is found to be a very important factor that governs the RTN immunity of the device.

II. Electrical Characterization Setup

The RTN measurements were performed on a 1T-1R structure comprising a TiN (BE)/HfO_2/Hf/TiN (TE) stack with 5 nm ALD HfO_2 and 10 nm Hf cap as the oxygen scavenging layer (Fig. 4(a)). After deposition, the HfO_2 was found to be mainly amorphous [**1**]. Considered device area were 40 nm × 40 nm with an integrated long channel MOSFET (W×L = 1×1 μm^2) directly connected to the cell to achieve precise compliance control during the breakdown percolative transient.

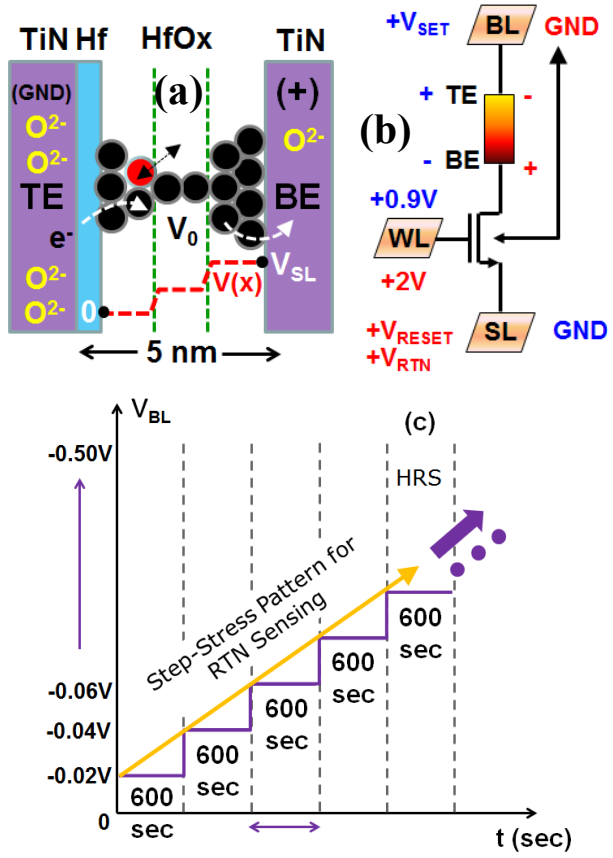

Figure 4. (a) RRAM stack comprising a TiN/HfO_x/Hf cap/TiN structure wherein the Hf cap is used as an effective oxygen scavenger (figure not drawn to scale). A typical shape of the conductive filament is shown to resemble an hourglass with the black circles representing the discrete vacancies. The oxygen ions stored in the TE / BE drift depending on the applied V_{BL} polarity. The red dotted line represents the unique QPC potential profile. (b) Typical polarity of voltages applied to the word line (WL), bit line (BL) and source line (SL) for SET (red), RESET and RTN (blue) measurements. The gate is fully opened for RTN sensing and partially closed for compliance-controlled SET. (c) Step-stress pattern for ultra-slow time domain RTN measurement with voltage steps of ΔV_{BL} = -20mV.

Forming / SET operation is initiated by applying positive DC sweep to the top electrode (TE) while limiting MOSFET drain current to 10-20μA by proper gate bias tuning. Conversely, RESET transition involves a negative DC sweep with MOSFET fully open. Unless otherwise stated, all RTN measurements in the HRS were carried out at negative sense voltage (V_{BL} < 0V → same as RESET polarity) using Keithley 2602 SMUs (Fig. 4(b)), so as to minimize the possibility of unintended SET transitions. Note that in our RTN tests, we apply a positive voltage to the source line (SL) and ground the bit line (BL) so as to more effectively turn-off the substrate - source/drain diode junctions in the transistor. To probe the voltage dependence of RTN, we employed a slow step-stress voltage test (Fig. 4(c)) wherein we begin with V_{BL} = -20 mV and for every 600 sec, the voltage is incremented by ΔV_{BL} = -20

mV. This very slow ramp rate (RR ~ 33μV/sec) ensures we are able to capture the RTN effects accurately in the time domain. We also carry out continuous slow ramped voltage tests in some cases for more time-efficient statistical data collection.

III. Field Distribution in the QPC Mode Filament

The conductive filament (CF) in the HRS has some unique features when operating in the QPC mode. A typical shape of the CF is illustrated in Fig. 5(a). The narrowest region of the CF is called the "*constriction*". While classical physics would suggest that a majority of the voltage would drop along this constriction as it is the narrowest section (given the inverse proportionality of resistance and area → $R \propto 1/Area$), considering the interference of incident and reflected electron waves at the filament-constriction (F-C) interface, a detailed quantum-level analysis [**20**] suggests that most of the voltage drops only at the two ends of the constriction and there is no voltage drop inside it (adiabatic transport regime). Assuming that the voltage drop away from the constriction is negligible (owing to high vacancy density), the effective applied V_{BL} ideally drops only at the two F-C interfaces. Knowing the fact that vacancy generation or recombination [**21**] – [**23**] and drift [**23**, **24**] are field-driven processes, the local ξ-field at the F-C interface is the key determinant of filament stability and RTN immunity.

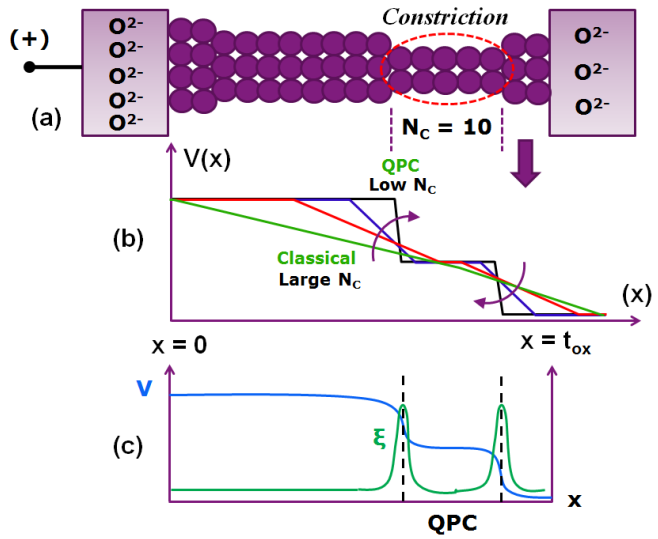

Figure 5. (a) Configuration of the oxygen vacancy CF in the HRS consisting of a narrow constriction with N_C number of defects (N_C = 10 in this illustration). (b) Approximate linearized potential profiles across the F-C region. As the defect count increases, the potential profile tends to become less abrupt and more uniform approaching the Ohmic regime. As reset gets deeper, the potential drops steeply within the sharper F-C interface. (c) Actual potential and local ξ-field profile along the F-C region. It is the local peak ξ-field that governs the susceptibility of the filament to vacancy perturbations.

In Figs. 5(b, c), we sketch the voltage and field distribution at the F-C interface for the cases of shallow and deep reset. As we get deeper in the reset phase, the potential drops over a much thinner F-C interface causing the localized ξ-field to magnify many times. This suggests that for the same external read voltage of V_{BL} = 0.1V, the internal localized field that can disturb the vacancies can be very different depending on the depth of reset. In our analysis, we assume the F-C properties to be symmetric at both ends so that ½ • V_{BL} voltage drop is taken at each interface. To our knowledge, there exists no straightforward analytical formula that can be applied to exactly compute the potential distribution profile in the QPC. Using some knowledge of the HRS *I-V* data (to determine the size, N_C, of the constriction) and an empirical model to describe the field intensification for lower values of N_C, the value of peak ξ-field can be roughly computed. Furthermore, we can also estimate the field [**25**] using our RTN tests (along with the thermochemical model) [**26**] by identifying the voltage level at which vacancies start to perturb the filament.

IV. RTN Analysis – Results and Discussion

A. Step-Stress RTN Analysis

Using the "ultra-slow" step-stress voltage profile in Fig. 4(c), the discrete current levels are identified for every 600 sec *I-t* trace at each V_{BL} value. These current levels are superposed on the modeled *I-V* traces using the QPC conduction model assuming different number of defects in the constriction (N_C), corresponding to a certain combination of electron wave frequencies, ω_X (indicative of length of constriction) and ω_Y (indicative of lateral width of constriction) [**6**, **7**]. The values of {ω_X = 8.6 × 10^{14} Hz, ω_Y = 9 × 10^{15} Hz} are chosen to best fit the measured data.

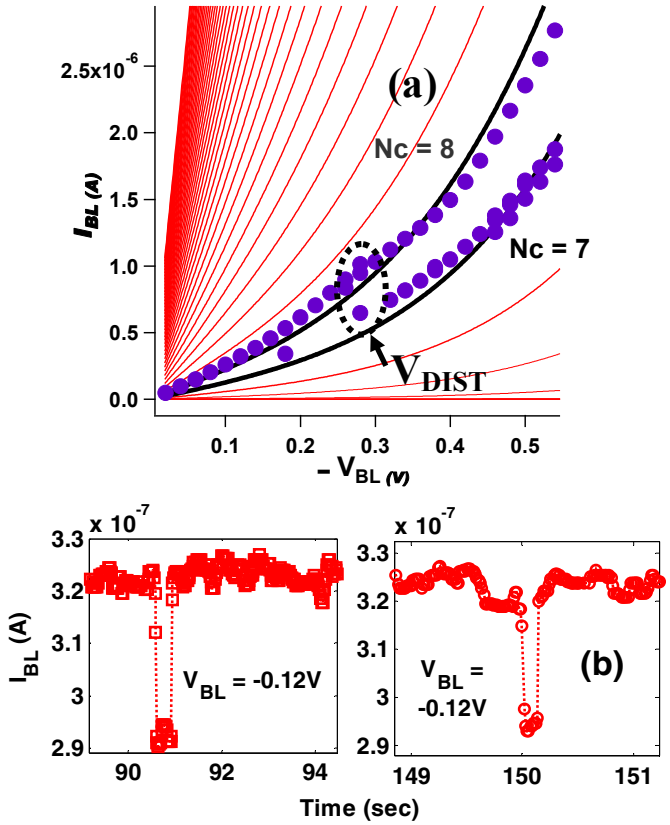

Figure 6. (a) Data points corresponding to discrete RTN current steps identified from measured long duration time domain noise signals, superposed on the *I-V* QPC traces modeled for various values of N_C starting from 1, for a given optimized combination of {ω_X, ω_Y} values. The measured current levels consistently fall on adjacent *I-V* traces for $|V_{BL}|$ > 0.28V. (b) Low voltage current traces even at $|V_{BL}|$ = 0.12V also exhibit RTN; however the current step (ΔI) is very small, possibly originating from the inelastic electron trap-detrap process.

Fig. 6(a) shows one such result wherein the current levels match one of the *I-V* traces very clearly, until about V_{BL} = -0.28V, when the points start to consistently fall on adjacent *I-V* lines corresponding to a change in the N_C value. It is this voltage we denote as the "disturb voltage (V_{DIST})", which refers to the minimum voltage needed to trigger the vacancy perturbations in the filament. It is obvious that the V_{DIST} would depend on the *RR* chosen, analogous to ramp rate dependence of the dielectric breakdown [**27**] and SET process [**28**].

It is important to note that different current levels are observed even for $|V_{BL}|$ << 0.28V, however, these levels are very close to each other (much lower than the difference in consecutive *I-V* lines) such that the points tend to merge on the plot in Fig. 6(a). As an example, we plot the *I-t* trace at V_{BL} = -0.12V in Fig. 6(b). Note the RTN trends at this voltage, which can only correspond to the charge trapping – detrapping process. Only the current fluctuations for $|V_{BL}| \geq$ 0.28V can be classified as V_0-induced RTN (trap-detrap contributions still exist, however they do not dominate the signal anymore). It is clear from the result here that the *I-V* model for QPC can be used as an effective tool to decouple the two RTN contributions and calibrate the behavior of vacancy perturbations separately, which is the focus of our study.

B. Voltage-Ramp RTN Analysis

Instead of the step-stress sequence, we may use the continuous voltage ramp as well to study the role of V_0 fluctuations. With higher resolution of current data superposed on the *I-V* traces as shown in Fig. 7, the V_{DIST} can be extracted more accurately here. The voltage ramp approach is more time-efficient and can be used to generate larger sets of data for statistical disturb trend analysis.

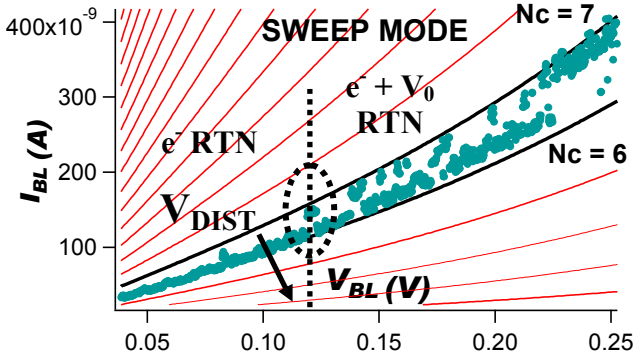

Figure 7. Plot of *I-V* voltage sweep data points on the QPC model traces to identify the V_{DIST} ~ 0.12V. Here, we use a positive polarity sweep to intentionally excite the disturb event. It is worth noting that the current levels in this plot are much lower than that in Fig. 6 due to a deeper reset level and the V_{DIST} value is correspondingly much lower. While the standard trapping – detrapping process always exists, the additional contribution of V_0-induced RTN sets in at $V_{BL} \geq V_{DIST}$.

C. Bimodal Time Constant Trends

For the RTN time-traces in Fig. 6, we used a statistical algorithm to extract the high-to-low and low-to-high current time constants ($\tau_{H\text{-}L}$, $\tau_{L\text{-}H}$) corresponding to the largest ΔI jumps for all values of $|V_{BL}|$. As plotted in Fig. 8, the slope or trend of the τ - V_{BL} relationship changes clearly at $|V_{BL}|$ = 0.28V. The different τ - V_{BL} dependency is an additional evidence supporting the concept of V_{DIST} when vacancy fluctuations begin to play a role affecting the disturb immunity. Detailed quantitative study on these bimodal τ - V_{BL} trends is an in-depth study of its own and is currently under investigation.

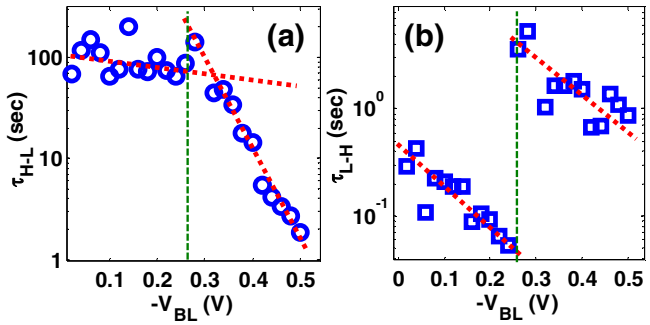

Figure 8. Extracted values of the time constant for the largest ΔI jumps observed in every 600 sec duration *I-t* data set in Fig. 6(a). The time constants corresponding to (a) high-to-low and (b) low-to-high current steps are indicated in this plot. In line with our previous discussion on the concept of V_{DIST}, we observe a completely different trend for τ at the same location where the current levels start to fall on different N_c levels in the *I-V* traces of Fig. 6(a). This double confims the presence of two distinct RTN phenomenon.

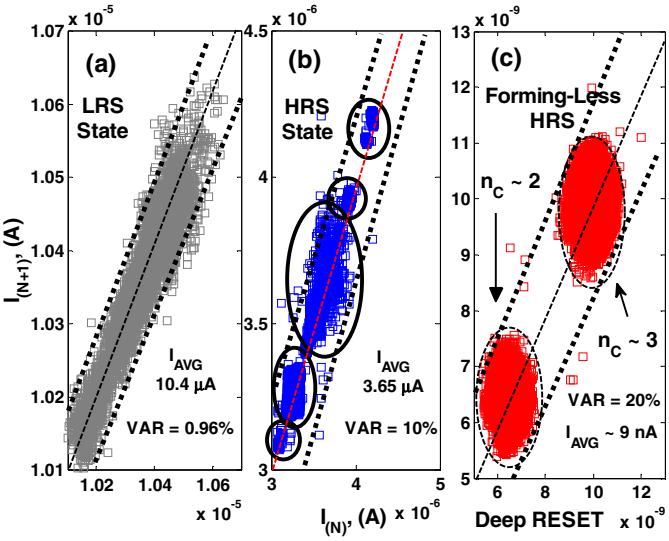

Figure 9. Scatter plot of consecutive current data measured during read disturb test at V_{READ} = 0.10V for (a) device in the SET state (LRS), (b) device in moderate RESET state (HRS) and (c) device in deep RESET state (observed here in a device which did not require forming and was in the LRS state to begin with). Widely spaced clusters are observed for HRS implying that variability and disturb immunity could get worse with deeper RESET.

D. RTN Variability in Different Resistance States

In order to assess the variability as a function of resistance state, we present a scatter plot of the consecutive current levels during RTN sensing (I_N, I_{N+1}) in Fig. 9 for three different scenarios – (a) LRS with large number of defects (R_{LRS} ~ 96kΩ), (b) post-forming HRS (R_{HRS} ~ 0.274MΩ) and (c) formingless device with R_{HRS} ~ 111MΩ (device was in the LRS to start with due to process-generated soft breakdown percolation path). We observe only one data cluster in the LRS (Fig. 9(a)) due to the existence of *1/f* noise (superposition of many *1/f²* Lorentzians each from a different trap in the dielectric) with very low variation of 0.96%. However, in the

HRS, (Fig. 9(b)), multiple clusters corresponding to RTN effect can be seen. These clusters are relatively close to each other with a variation ~ 10%. It is the last scatter plot (Fig. 9(c)) that shows substantial variation > 20% with two very distinct clusters and very low current values in the nano-ampere range. As we move to deeper resistance states, the contribution of single traps becomes more phenomenal resulting in significant variations at read conditions. The formingless device enabled us to go to deeper reset states probably because the filament created during fabrication was small in defect count and passivating just a few defects may result in a narrow linear chain of vacancies comprising the constriction, leading to very high resistance. It is to be noted that even for such low I_{READ} ~ 6-9nA ($|V_{BL}|$ = 0.1V), we are still operating in the QPC mode without any filamentary rupture, as will be evident from our discussions relating to Fig. 13 in Section IV.G.

E. Effect of Reset Stop Voltage on Variability

While increasing the reset voltage may initially help in passivating more defects and reducing filament conductivity further starting from LRS, application of too high a reset voltage may result in a situation wherein there are no more ions / vacancies available for recombination and the stress is sufficient enough to trigger additional defect generation.

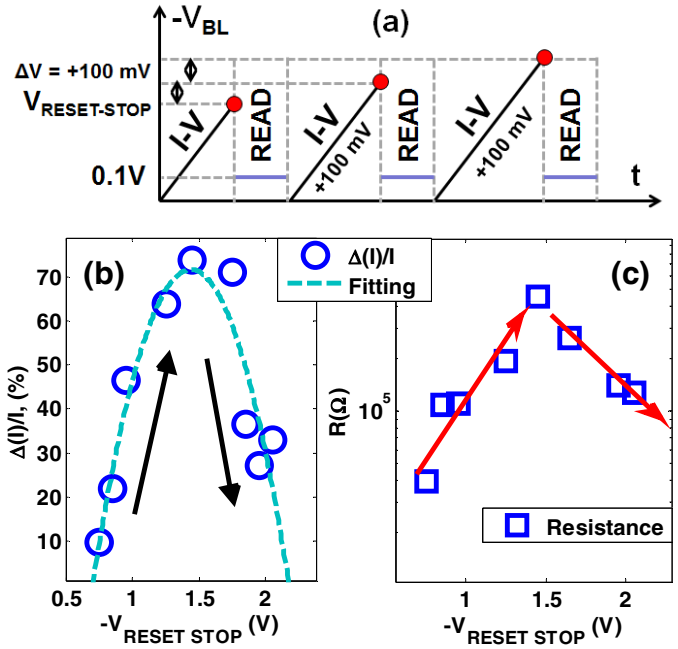

Figure 10. (a) Testing scheme used to probe the effect of maximum reset voltage ($V_{RESET\text{-}STOP}$) on the variability in HRS. The standard read condition of $|V_{READ}|$ = 0.10V is used to extract ($\Delta I/I$) and filament resistance values. Trends of (b) ($\Delta I/I$) and (c) R show a peak at V_{RESET} ~ -1.5V, which provides the maximum reset depth. Further increase in V_{RESET} results in additional defect generation causing ($\Delta I/I$) and R to go down.

It is therefore essential to determine the optimum reset voltage ($V_{RESET\text{-}STOP}$), so that we achieve the largest memory window. We use the simple technique in Fig. 10(a) where we increment $V_{RESET\text{-}STOP}$ by 100mV each time sweeping from 0V and then extract the ($\Delta I/I$) value from I-t traces at V_{READ} = -0.1V. Figs. 10(b, c) plot the ($\Delta I/I$) and filament resistance (R) values as a function of $V_{RESET\text{-}STOP}$. We observe a peak in the relative noise amplitude as well as filament resistivity at around -1.5V, which corresponds to the lowest value of N_C that can be achieved (lower N_C → larger $\Delta I/I$). When V_{RESET} is increased beyond 1.5V, ($\Delta I/I$, R) drop again due to additional defect generation. Using this approach, we identify the optimum value of $|V_{RESET\text{-}STOP}|$ ~ 1.5V for this HfO_x stack. The balance between competing defect generation and recombination processes is therefore a very important aspect to consider for tuning the switching parameters in RRAM.

F. Summary of RTN Signatures Observed

After the reset transition, when RTN measurements are performed, we generally expect to see steady-state fluctuations as illustrated in Fig. 11(a). However, as the sense voltage is increased, it may be possible for the device to go to deeper metastable HRS states (Fig. 11(b)) or degrade to shallower HRS states (Fig. 11(c)) triggered by vacancy generation during the prolonged sense measurements. It is necessary to identify these anomalous trends while studying the RTN phenomenon.

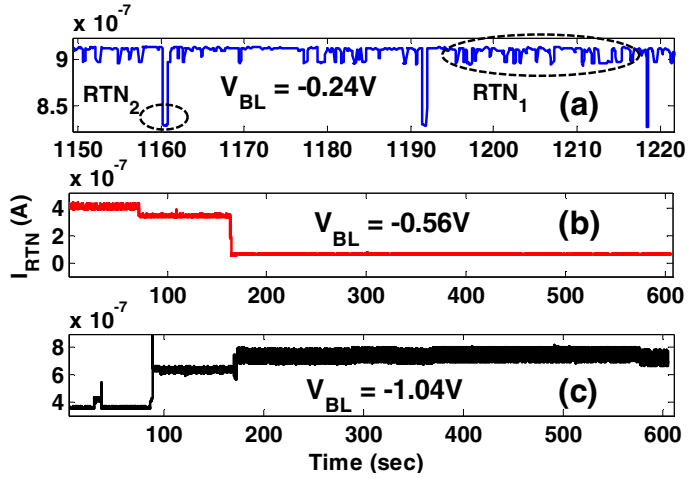

Figure 11. Different RTN signature trends observed in the HRS of a single device for various V_{BL} values. (a) Steady-state embedded RTN with multiple components corresponding to vacancy and multiple trap/detrap contributions. (b) Monotonic step wise decrease in current due to deeper reset of the filament (additional passivation / movement of a defect out of the constriction). (c) Monotonic step wise increase in current due to stress-induced structural perturbations of the constriction. During the measurements for (b, c), there is a physical change in the shape and/or size of the filament constriction.

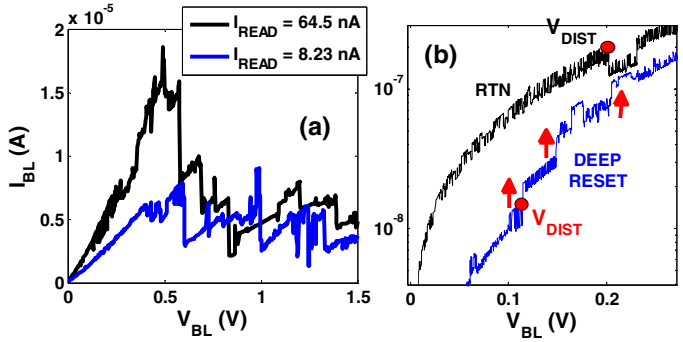

Figure 12. (a) I-V trace during reset for two different switching cycles with shallow (I_{READ} ~ 64.5 nA) and deep reset (I_{READ} ~ 8.23 nA). (b) Corresponding slow ramp sweep disturb test that indicates a much lower V_{DIST} ~ 0.12V for the case of deeper reset device. The value of V_{DIST} seems to be very sensitive to the depth of reset. It also depends on the speed of ramping measurement, which is a topic that deserves a separate in-depth study.

G. RTN Immunity and Reset Depth Dependence

As discussed in the previous sub-sections, the reset depth has a significant effect on the stability of the filament. This is more apparent in the slow HRS *I-V* sweeps in Fig. 12(b) corresponding to shallow and deep reset cases with read currents, I_{READ} ~ 64.5nA and 8.23nA respectively. The reset trends for these two devices are shown in Fig. 12(a). As we reset deeper, the constriction becomes narrower (higher ω_Y). For the same applied V_{BL}, the local ξ-field at the F-C interface can be enhanced several times for a deep reset, which makes the filament highly prone to unintended set or disturb event, leading to erroneous read.

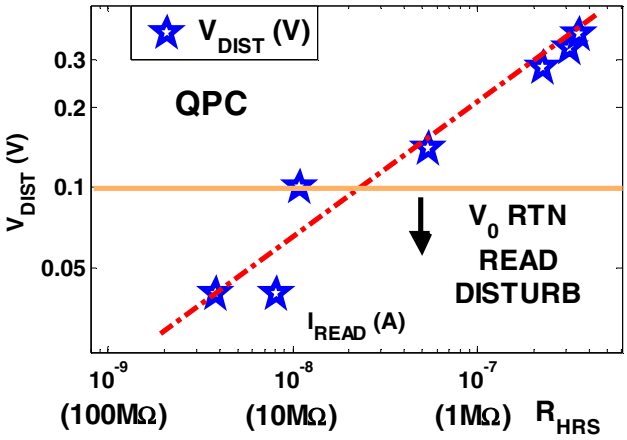

Figure 13. Plot of V_{DIST} versus I_{READ} for various levels of reset. The V_{DIST} here is identified from the step-stress RTN tests at a very slow ramp rate (RR) ~ 33.3 μV/sec. Clearly, we observe a lower V_{DIST} for deeper reset levels, which is due to field intensification at the F-C interface for lower N_c values in the constriction. For very deep reset, it is possible to encounter situations of V_{DIST} < V_{READ} = 0.1V, in which case, we end up with very poor disturb immunity.

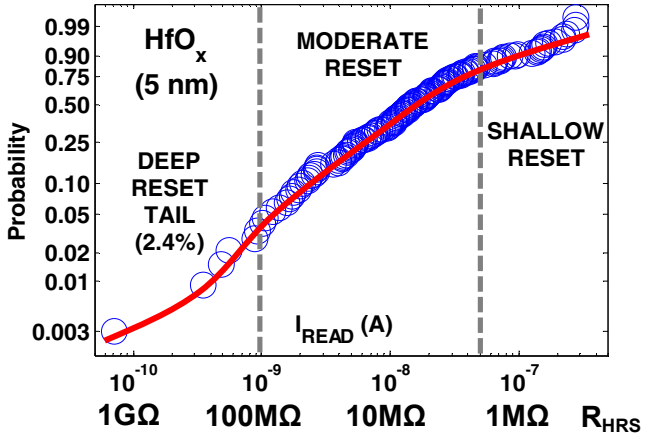

Figure 14. Read current distribution plot for many cycles of switching on many similar HfO_x devices. It is hard to observe very deep reset in HfO_x. Only 2.4% of the measurements result in sub nanoampere I_{READ}. It appears difficult to cause the filament to rupture, as confirmed by our V_{DIST} measurements in Fig. 13.

We plot a trend of V_{DIST} as a function of I_{READ} for several switching cycles in a device (Fig. 13). The trend of lower V_{DIST} for lower I_{READ} is an indirect evidence that supports our hypothesis of QPC-mode operation [**6**, **7**]. This is because, if the filament were to rupture resulting in a tunneling barrier, then thicker barriers (lower I_{READ}) would cause a more gradual potential gradient ($\downarrow\xi$) implying higher $V_{DIST,}$ which is not supported by our experimental data. Even for I_{READ} ~ 1-10nA, the V_{DIST} - I_{READ} relationship is monotonic with positive slope, implying that we are still operating in the QPC regime.

Therefore, as far as the HfO_x stack is concerned, the QPC conduction best describes the HRS state. It is worth noting that achieving deep reset is quite a rare event for HfO_x, as the read current tail in Fig. 14 shows. Similar RTN studies on other stacks such as AlO_x, bilayer HfO_x-AlO_x are currently under way to find out whether these stacks also reset to the QPC mode or undergo substantial filament rupture resulting in a tunneling barrier. Initial studies show that the tunneling mode may be more immune to RTN effects due to the potential redistributing across the barrier region which may be much thicker than the F-C interface width.

V. Conclusion

In this study, we have presented a comprehensive analysis on the susceptibility of the conductive filament in HfO_x to RTN induced by vacancy perturbations. We were able to decouple the role of trapping-detrapping from V_0-RTN. The key findings may be summarized as follows.

- While the operation of Flash memory is governed only by one RTN mechanism (standard carrier trap / detrap), RRAM devices experience an additional more dominant contribution to noise from V_0 fluctuations in the filament.
- High resistance state in HfO_x is best described by the QPC mode of conduction as we seldom observe very deep reset (filament rupture).
- For the QPC mode, the deeper the reset level, the lower the value of V_{DIST}. The immunity to RTN is mainly determined by the width of the filament-constriction interface.
- It is possible to have an unstable filament and low immunity to disturb events even at V_{READ} = 0.1V, if the reset is deep but not deep enough to induce a filament rupture.
- The shape and size of the filament determine the QPC potential profile and in turn the magnitude of RTN. For improved immunity to RTN, the filament shape and size need to be engineered using a controlled forming process.
- There exists an optimum reset voltage to reach the deepest reset state. The extent of reset should be determined not just by the memory window, but also by the probability of observing vacancy perturbations at the deep reset state.
- The HfO_x stack does not have a very stable filament in the HRS. Other dielectric materials are currently under study and the material properties impacting RTN need to be precisely identified.

Further quantitative statistical analysis is currently under way to model the time constant trends and dependence of V_{DIST} on RR using the fundamental mechanisms of vacancy diffusion / drift and generation / recombination for V_0-triggered RTN. The results of the model being developed and a comparison of RTN in different dielectric stacks will be presented elsewhere in the near future.

REFERENCES

[1] B. Govoreanu, G.S. Kar, Y.Y. Chen, V. Paraschiv, S. Kubicek, A. Fantini, I.P. Radu, L. Goux, S. Clima, R. Degraeve, N. Jossart, O. Richard, T. Vandeweyer, K. Seo, P. Hendrickx, G. Pourtois, H. Bender, L. Altimime, D.J. Wouters, J.A. Kittl and M. Jurczak, "10×10 nm^2 Hf/HfO_x crossbar resistive RAM with excellent performance, reliability and low-energy operation", *IEEE International Electron Devices Meeting (IEDM),* pp.31.6.1 - 31.6.4, (2011).

[2] Y.Y. Chen, B. Govoreanu, L. Goux, R. Degraeve, A. Fantini, G.S. Kar, D.J. Wouters, G. Groeseneken, J.A. Kittl, M. Jurczak and L. Altimime, "Balancing SET/RESET Pulse for $>10^{10}$ Endurance in HfO_2/Hf 1T1R Bipolar RRAM", *IEEE Transactions on Electron Devices,* Vol.59, No.12, pp.3243-3249, (2012).

[3] B. Butcher, S. Koveshnikov, D.C. Gilmer, G. Bersuker, M.G. Sung, A. Kalantarian, C. Park, R. Geer, Y. Nishi, P.D. Kirsch and R. Jammy, "High endurance performance of 1T1R HfO_x based RRAM at low (<20μA) operative current and elevated (150°C) temperature", *IEEE Integrated Reliability Workshop Final Report (IIRW),* pp.146-150, (2011).

[4] H.Y. Lee, P.S. Chen, T.Y. Wu, Y.S. Chen, C.C. Wang, P.J. Tzeng, C.H. Lin, F. Chen, C.H. Lien and M.J. Tsai, "Low power and high speed bipolar switching with a thin reactive Ti buffer layer in robust HfO2 based RRAM", *IEEE International Electron Devices Meeting (IEDM),* pp. 1-4, (2008).

[5] B. Chen, B. Gao, S.W. Sheng, L.F. Liu, X.Y. Liu, Y.S. Chen, Y. Wang, R.Q. Han, B. Yu and J.F. Kang, "A Novel Operation Scheme for Oxide-Based Resistive-Switching Memory Devices to Achieve Controlled Switching Behaviors", *IEEE Electron Device Letters,* Vol. 32, No. 3, pp.282-284, (2011).

[6] R. Degraeve, P.J. Roussel, L. Goux, D.J. Wouters, J.A. Kittl, L. Altimime, M. Jurczak and G. Groeseneken, "Generic learning of TDDB applied to RRAM for improved understanding of conduction and switching mechanism through multiple filaments", *IEEE International Electron Devices Meeting (IEDM),* pp.28.4.1-28.4.4, (2010).

[7] R. Degraeve, L. Goux, S. Clima, B. Govoreanu, Y.Y. Chen, G.S. Kar, P.J. Roussel, G. Pourtois, D.J. Wouters, L. Altimime, M. Jurczak, G. Groeseneken and J.A. Kittl, "Modeling and tuning the filament properties in RRAM metal oxide stacks for optimized stable cycling", *International Symposium on VLSI Technology, Systems, and Applications (VLSI-TSA),* pp.1-2, (2012).

[8] R. Degraeve, A. Fantini, S. Clima, B. Govoreanu, L. Goux, Y.Y. Chen, D.J. Wouters, P.J. Roussel, G.S. Kar, G. Pourtois, S. Cosemans, J.A. Kittl, G. Groeseneken, M. Jurczak and L. Altimime, "Dynamic 'hour glass' model for SET and RESET in HfO_2 RRAM", *Symposium on VLSI Technology (VLSIT),* pp.75-76, (2012).

[9] R. Degraeve *et. al.*, *IEEE Transactions on Electron Devices*, Manuscript under preparation, (2013).

[10] C.M. Chang, S.S. Chung, Y.S. Hsieh, L.W. Cheng, C.T. Tsai, G.H. Ma, S.C. Chien and S.W. Sun, "The observation of trapping and detrapping effects in high-κ gate dielectric MOSFETs by a new gate current Random Telegraph Noise (I_G-RTN) approach", *IEEE International Electron Devices Meeting (IEDM),* pp.1-4, (2008).

[11] K. Fukuda, Y. Shimizu, K. Amemiya, M. Kamoshida, C. Hu, "Random telegraph noise in flash memories - model and technology scaling", *IEEE International Electron Devices Meeting (IEDM),* pp.169-172, (2007).

[12] A. Ghetti, C.M. Compagnoni, F. Biancardi, A.L. Lacaita, S. Beltrami, L. Chiavarone, A.S. Spinelli and A. Visconti, "Scaling trends for random telegraph noise in deca-nanometer Flash memories", *IEEE International Electron Devices Meeting (IEDM),* pp.1-4, (2008).

[13] F.M. Puglisi, P. Pavan, A. Padovani, L. Larcher and G. Bersuker, "Random telegraph signal noise properties of HfO_x RRAM in high resistive state", *Proceedings of the European Solid-State Device Research Conference (ESSDERC),* pp.274-277, (2012).

[14] M. Terai, Y. Sakotsubo, Y. Saito, S. Kotsuji and H. Hada, "Memory-state dependence of random telegraph noise of Ta_2O_5/TiO_2 stack ReRAM", *IEEE Electron Device Letters,* Vol. 31, No. 11, pp. 1302-1304, (2010).

[15] Y.H. Tseng, W.C. Shen, C.E. Huang, C.J. Lin and Y.C. King, "Electron trapping effect on the switching behavior of contact RRAM devices through random telegraph noise analysis", *IEEE International Electron Devices Meeting (IEDM)*, pp.28.5.1 - 28.5.4, (2010).

[16] J.K. Lee, J.W. Lee, J. Park, S.W. Chung, J.S. Roh, S.J. Hong, I.W. Cho, H.I. Kwon and J.H. Lee, "Extraction of trap location and energy from random telegraph noise in amorphous TiO_x resistance random access memories", *Applied Physics Letters*, Vol. 98, 143502, (2011).

[17] D. Ielmini, F. Nardi and C. Cagli, "Resistance-dependent amplitude of random telegraph-signal noise in resistive switching memories", *Applied Physics Letters*, Vol. 96, 053503, (2010).

[18] D. Veksler, G. Bersuker, B. Chakrabarti, E. Vogel, S. Deora, K. Matthews, D.C. Gilmer, H.F. Li, S. Gausepohl and P.D. Kirsch, "Methodology for the statistical evaluation of the effect of random telegraph noise (RTN) on RRAM characteristics", *IEEE International Electron Devices Meeting (IEDM)*, pp.9.6.1 – 9.6.4, (2012).

[19] M. Sasaki, "An electron conduction model of resistive memory for resistance dispersion, fluctuation, filament structures, and Set/Reset mechanism", *Journal of Applied Physics*, Vol. 112, 014501, (2012).

[20] S. Ulreich and W. Zwerger, "Where is the potential drop in a quantum point contact?", *Superlattices and Microstructures*, Vol. 23, Issues 3–4, pp. 719-730, (1998).

[21] G. Bersuker, A. Korkin, L. Fonseca, A. Safonov, A. Bagatur'yants and H.R. Huff, "The role of localized states in the degradation of thin gate oxides", *Microelectronic Engineering*, Vol. 69, Issues 2–4, pp. 118-129, (2003).

[22] J.W. McPherson, J. Kim, A. Shanware, H. Mogul and J. Rodriguez, "Trends in the ultimate breakdown strength of high dielectric-constant materials", *IEEE Transactions on Electron Devices,* Vol.50, No.8, pp. 1771- 1778, (2003).

[23] L. Larcher, A. Padovani, O. Pirrotta, L. Vandelli, and G. Bersuker, "Microscopic understanding and modeling of HfO_2 RRAM device physics", *IEEE International Electron Devices Meeting (IEDM)*, pp. 474-477, (2012).

[24] D.B. Strukov and R.S. Williams, "Exponential ionic drift: fast switching and low volatility of thin-film memristors", *Applied Physics A*, Vol. 94, Issue 3, pp.515-519, (2009).

[25] N. Raghavan, R. Degraeve, A. Fantini, L. Goux, D.J. Wouters, G. Groeseneken and M. Jurczak, "Modeling the impact of reset depth on vacancy induced filament perturbations in HfO_2 RRAM", *IEEE Electron Device Letters*, Under Review, (2013).

[26] J.W. McPherson, J.Y. Kim, A. Shanware and H. Mogul, "Thermochemical description of dielectric breakdown in high dielectric constant materials", *Applied Physics Letters*, Vol. 82(13), pp.2121-2123, (2003).

[27] A. Kerber, L. Pantisano, A. Veloso, G. Groeseneken, M. Kerber, "Reliability screening of high-κ dielectrics based on voltage ramp stress", *Microelectronics Reliability*, Vol. 47, Issues 4–5, pp. 513-517, (2007).

[28] A. Fantini, D.J. Wouters, R. Degraeve, L. Goux, L. Pantisano, G.S. Kar, Y.Y. Chen, B. Govoreanu, J.A. Kittl, L. Altimime and M. Jurczak, "Intrinsic switching behavior in HfO_2 RRAM by fast electrical measurements on novel 2R test structures", *4th IEEE International Memory Workshop (IMW),* pp.45-48, (2012).